Emission and excitation contributions to enhanced single molecule fluorescence by gold nanometric apertures

Jérôme Wenger,[1*] **Davy Gérard,**[1] **José Dintinger,**[2] **Oussama Mahboub,**[2] **Nicolas Bonod,**[1] **Evgeny Popov,**[1] **Thomas W. Ebbesen,**[2] **and Hervé Rigneault**[1]

[1] *Institut Fresnel, Aix-Marseille Université, CNRS, Campus de St Jérôme, 13397 Marseille, France*

[2] *Institut de Science et Ingénierie Supramoléculaires, Université Louis Pasteur, CNRS, 8 allée G. Monge, 67000 Strasbourg, France*

[*] *Corresponding author: jerome.wenger@fresnel.fr*

www.fresnel.fr/mosaic

Abstract: We detail the role of single nanometric apertures milled in a gold film to enhance the fluorescence emission of Alexa Fluor 647 molecules. Combining fluorescence correlation spectroscopy and lifetime measurements, we determine the respective contributions of excitation and emission in the observed enhanced fluorescence. We characterize a broad range of nanoaperture diameters from 80 to 310 nm, and highlight the link between the fluorescence enhancement and the local photonic density of states. These results are of great interest to increase the effectiveness of fluorescence-based single molecule detection and to understand the interaction between a quantum emitter and a nanometric metal structure.

OCIS codes: (050.1220) Apertures; (240.6680) Surface plasmons; (170.6280) Spectroscopy, fluorescence and luminescence; (160.4236) Nanomaterials

References and links

1. W. L. Barnes, "Fluorescence near interfaces: the role of photonic mode density," J. Mod. Opt. **45**, 661-699 (1998).
2. J. R. Lakowicz, "Radiative decay engineering 5: metal-enhanced fluorescence and plasmon emission," Anal. Biochem. **337**, 171-194 (2005).
3. E. Fort and S. Grésillon, "Surface enhanced fluorescence," J. Phys. D: Appl. Phys. **41**, 013001 (2008).
4. P. Anger, P. Bharadwaj and L. Novotny, "Enhancement and Quenching of Single-Molecule Fluorescence," Phys. Rev. Lett. **96**, 113002 (2006).
5. S. Kühn, U. Håkanson, L. Rogobete and V. Sandoghdar, "Enhancement of Single-Molecule Fluorescence using a Gold Nanoparticle as an Optical Nanoantenna," Phys. Rev. Lett. **97**, 017402 (2006).
6. J. Zhang, Y. Fu, M. H. Chowdhury, and J. R. Lakowicz, "Metal-Enhanced Single-Molecule Fluorescence on Silver Particle Monomer and Dimer: Coupling Effect between Metal Particles," Nano Lett. **7**, 2101-2107 (2007).
7. S. Gerber, F. Reil, U. Hohenester, T. Schlagenhaufen, J. R. Krenn, and A. Leitner, "Tailoring light emission properties of fluorophores by coupling to resonance-tuned metallic nanostructures," Phys. Rev. B **75**, 073404 (2007).
8. Y. Zhang, K. Aslan, M. J. R. Previte, and C. D. Geddes, "Metal-enhanced fluorescence: Surface plasmons can radiate a fluorophore's structured emission," Appl. Phys. Lett. **90**, 053107 (2007).
9. F. Tam, G. P. Goodrich, B. R. Johnson, and N. J. Halas, "Plasmonic Enhancement of Molecular Fluorescence," Nano Lett. **7**, 496-501 (2007).
10. J. Enderlein and T. Ruckstuhl, "The efficiency of surface-plasmon coupled emission for sensitive fluorescence detection," Opt. Express **13**, 8855-8865 (2005).

#92310 - $15.00 USD Received 31 Jan 2008; revised 15 Feb 2008; accepted 15 Feb 2008; published 20 Feb 2008

11. J. N. Farahani, D. W. Pohl, H.-J. Eisler, and B. Hecht, "Single Quantum Dot Coupled to a Scanning Optical Antenna: A Tunable Superemitter," Phys. Rev. Lett. **95**, 017402 (2005).
12. O. L. Muskens, V. Giannini, J. A. Sanchez-Gil, and J. Gomez Rivas, "Strong Enhancement of the Radiative Decay Rate of Emitters by Single Plasmonic Nanoantennas," Nano Lett. **7**, 2871-2875 (2007).
13. J. S. Biteen, D. Pacifici, N. S. Lewis and H. A. Atwater, "Enhanced Radiative Emission Rate and Quantum Efficiency in Coupled Silicon Nanocrystal-Nanostructured Gold Emitters," Nano Lett. **5**, 1768-1773 (2005).
14. G. L. Liu, J. Kim, and L. P. Lee, "Fluorescence enhancement of quantum dots enclosed in Au nanopockets with subwavelength aperture," Appl. Phys. Lett. **89**, 241118 (2006).
15. Y.-J. Hung, I. I. Smolyaninov, C. C. Davis and H.-C. Wu, "Fluorescence enhancement by surface gratings," Opt. Express **14**, 10825-10830 (2006).
16. G. Sun, J. B. Khurgin and R. A. Soref, "Practicable enhancement of spontaneous emission using surface plasmons," Appl. Phys. Lett. **90**, 111107 (2007).
17. Y. Liu and S. Blair, "Fluorescence enhancement from an array of subwavelength metal apertures," Opt. Lett. **28**, 507-509 (2003).
18. A. G. Brolo, S. C. Kwok, M. D. Cooper, M. G. Moffitt, C.-W. Wang, R. Gordon, J. Riordon, and K. L. Kavanagh, "Surface Plasmon-Quantum Dot Coupling from Arrays of Nanoholes," J. Phys. Chem. B **110**, 8307-8313 (2006).
19. J. H. Kim and P. J. Moyer, "Laser-induced fluorescence within subwavelength metallic arrays of nanoholes indicating minimal dependence on hole periodicity," Appl. Phys. Lett. **90**, 131111 (2007).
20. U. C. Fischer, "Submicrometer aperture in a thin metal film as a probe of its microenvironment through enhanced light scattering and fluorescence," J. Opt. Soc. Am. B **3**, 1239-1244 (1986).
21. H. Rigneault, J. Capoulade, J. Dintinger, J. Wenger, N. Bonod, E. Popov, T. W. Ebbesen and P.-F. Lenne, "Enhancement of Single-Molecule Fluorescence Detection in Subwavelength Apertures," Phys. Rev. Lett. **95**, 117401 (2005).
22. J. Wenger, B. Cluzel, J. Dintinger, N. Bonod, A.- L. Fehrembach, E. Popov, P.-F. Lenne, T. W. Ebbesen, and H. Rigneault, "Radiative and Nonradiative Photokinetics Alteration Inside a Single Metallic Nanometric Aperture," J. Phys. Chem. C **111**, 11469-11474 (2007).
23. D. Gérard, J. Wenger, N. Bonod, E. Popov, H. Rigneault, F. Mahdavi, S. Blair, J. Dintinger, and T. W. Ebbesen, "Nanoaperture-enhanced fluorescence: Towards higher detection rates with plasmonic metals," Phys. Rev. B **77**, 045413 (2008).
24. H. G. Craighead, "Future lab-on-a-chip technologies for interrogating individual molecules," Nature (London) **442**, 387-393 (2006).
25. J. T. Mannion, and H. G. Craighead, "Nanofluidic Structures for Single Biomolecule Fluorescent Detection," Biopolymers **85**, 131-143 (2006).
26. C. Genet and T. W. Ebbesen, "Light in tiny holes," Nature (London) **445**, 39-46 (2007).
27. M. J. Levene, J. Korlach, S. W. Turner, M. Foquet, H. G. Craighead, and W. W. Webb, "Zero-Mode Waveguides for Single-Molecule Analysis at High Concentrations," Science **299**, 682-686 (2003).
28. K. T. Samiee, M. Foquet, L. Guo, E. C. Cox, H. G. Craighead, "Lambda repressor oligomerization kinetics at high concentrations using fluorescence correlation spectroscopy in zero-mode waveguides," Biophys. J. **88**, 2145-2153 (2005).
29. M. Leutenegger, M. Gösch, A. Perentes, P. Hoffmann, O. J. F. Martin, T. Lasser, "Confining the sampling volume for Fluorescence Correlation Spectroscopy using a sub-wavelength sized aperture," Opt. Express **14**, 956-969 (2006).
30. J. Wenger, F. Conchonaud, J. Dintinger, L. Wawrezinieck, T. W. Ebbesen, H. Rigneault, D. Marguet, P. F. Lenne, "Diffusion Analysis within Single Nanometric Apertures Reveals the Ultrafine Cell Membrane Organization," Biophys. J. **92**, 913-919 (2007).
31. J. Wenger, D. Gérard, P.-F. Lenne, H. Rigneault, J. Dintinger, T. W. Ebbesen, A. Boned, F. Conchonaud, D. Marguet, "Dual-color fluorescence cross-correlation spectroscopy in a single nanoaperture : towards rapid multicomponent screening at high concentrations," Opt. Express **14**, 12206-12216 (2006).
32. J. Widengren, R. Rigler, and U. Mets, "Triplet-state monitoring by fluorescence correlation spectroscopy," J. Fluoresc. **4**, 255-258 (1994).
33. J. Widengren, U. Mets, and R. Rigler, "Fluorescence correlation spectroscopy of triplet states in solution: a theoretical and experimental study," J. Phys. Chem. **99**, 13368-13379 (1995).
34. V. Buschmann, K. D. Weston, and M. Sauer, "Spectroscopic Study and Evaluation of Red-Absorbing Fluorescent Dyes," Bioconjugate Chem. **14**, 195-204 (2003).
35. J. Widengren and P. Schwille, "Characterization of Photoinduced Isomerization and Back-Isomerization of the Cyanine Dye Cy5 by Fluorescence Correlation Spectroscopy," J. Phys. Chem. A **104**, 6416-6428 (2000).
36. C. Zander, J. Enderlein and R. A. Keller (Eds.), *Single-Molecule Detection in Solution - Methods and Applications*, (VCH-Wiley, Berlin/New York, 2002).
37. F. Mahdavi, Y. Liu, and S. Blair, "Modeling Fluorescence Enhancement from Metallic Nanocavities," Plasmonics **2**, 129-142 (2007).
38. E. Popov, M. Nevière, J. Wenger, P.-F. Lenne, H. Rigneault, P. Chaumet, N. Bonod, J. Dintinger, T. W. Ebbesen, "Field enhancement in single subwavelength apertures," J. Opt. Soc. Am. A **23**, 2342-2348 (2006).

#92310 - $15.00 USD Received 31 Jan 2008; revised 15 Feb 2008; accepted 15 Feb 2008; published 20 Feb 2008

1. Introduction

The fluorescence emission of a single molecule can be enhanced by properly tailoring its photonic environment, leading to new opportunities for single molecule detection. The environment can affect the fluorescence emission in three ways: (i) by locally enhancing the excitation intensity, (ii) by increasing the emitter's radiative rate and quantum efficiency, and (iii) by modifying its radiation pattern, towards a higher emission directionality to the detectors. Determining the influence of these processes is a crucial issue to characterize nanodevices for enhanced fluorescence, which has been a topic of great interest for the last decade [1, 2, 3].

In the growing field of nanostructure-enhanced fluorescence, much attention is currently devoted to metal structures, where surface plasmons can play an additional role [2, 3]. For instance, recent studies involve metallic nanoparticles [4, 5, 6, 7, 8], core-shell particles [9], thin films [10], nanoantennas [11, 12], nanoporous gold [13], nanopockets [14], metallic gratings [15, 16], nanoaperture arrays [17, 18, 19], and single nanoapertures [20, 21]. For all these geometries, determining the specific influence of a nanostructure on the fluorescence emission remains a challenging task, as the detected signal results from a product of excitation and emission processes. Excitation depends on the interaction between the driving field and the nanostructure, while at moderate optical powers, the emission efficiency is set by the balance of radiative and non-radiative decays and the modification of the radiation pattern.

In this paper, we discuss the fluorescence alteration induced by a single nanometric aperture milled in a gold film with diameters ranging from 80 to 310 nm. Fluorescence correlation spectroscopy (FCS) is combined with fluorescence lifetime measurements on the same setup to characterize the photokinetic rates of Alexa Fluor 647 molecules inside the nanoapertures. Compared to previous studies [21, 22, 23], we now quantitatively detail the contributions of excitation and emission enhancements in the reported fluorescence gain for a broad range of aperture diameters, and relate these effects to the alteration of the local density of states [1].

In spite of their conceptual simplicity, nanoapertures bear appealing properties to increase the effectiveness of fluorescence-based single-molecule detection [24, 25, 26]. Thanks to these devices, a large range of biologic processes can be efficiently monitored with single molecule resolution at micromolar concentrations [27, 28, 29]. The use of nanoaperture for biophotonics applications can also be extended to the investigation of live cell membranes [30] and dual-labels cross-correlation studies [31]. Therefore, understanding the fluorescence alteration in a nanoaperture is of practical importance for high-efficiency single-molecule analysis.

The paper is outlined as follows. In Section 2, we describe the procedure used to characterize the different photokinetic rates. Section 3 presents the experimental methods used throughout the paper. Results on the fluorescence detection rates and lifetimes are presented in Section 4 for aperture diameters ranging from 80 to 310 nm. In Section 5, we combine the experimental results to detail the fluorescence photokinetics alteration and assess the respective role of excitation and emission enhancements in the fluorescence process. Finally, we summarize our conclusions in Section 6.

2. Fluorescence characterization procedure

To introduce our characterization procedure in a few words, we implement FCS to reliably quantify the detected number of molecules and the fluorescence count rate per molecule *CRM*, which is recorded as the excitation power I_e is raised. Global analysis of the *CRM* vs. I_e curve, combined to lifetime measurements using time correlated single photon counting (TCSPC) alongside the FCS setup, gives the relative contribution of emission and excitation gains in the overall fluorescence enhancement, in a similar trend as in references [32, 33]. We point out that this characterization procedure combining FCS and TCSPC can be straightforwardly extended to other types of plasmonic nanostructures.

#92310 - $15.00 USD Received 31 Jan 2008; revised 15 Feb 2008; accepted 15 Feb 2008; published 20 Feb 2008

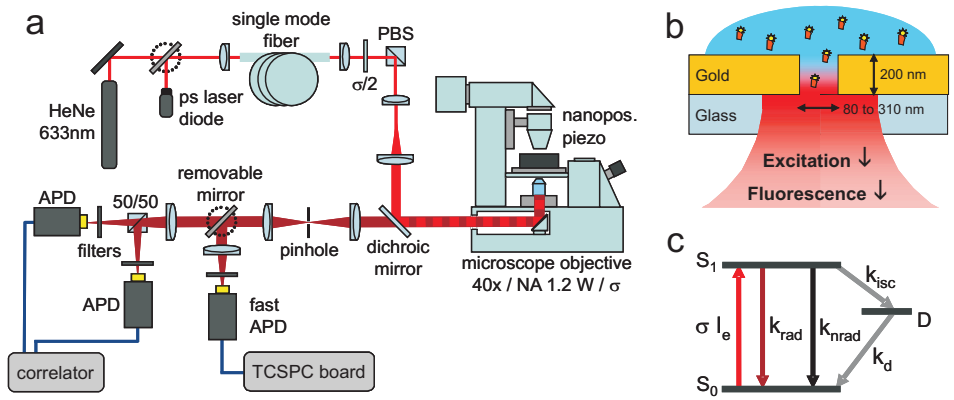

Fig. 1. (a) Schematic view of the experimental setup combining FCS and TCSPC. (b) Nanoaperture configuration. (c) Notations used to describe the molecular transition rates.

We introduce the fluorescence enhancement η_F in a nanoaperture as the ratio of the detected fluorescence rate per molecule in the aperture CRM_{aper} and in open solution CRM_{sol} at a fixed excitation power, that is $\eta_F = CRM_{aper}/CRM_{sol}$. To understand the physical origin of the increase in the fluorescence brightness already reported in [23], we begin by expressing the fluorescence rate per molecule CRM. Throughout this paper, we treat Alexa Fluor 647 as a three energy levels system, as illustrated in Fig. 1(c). S_0 denotes the ground state, S_1 the excited singlet state and D is a dark (non-fluorescent) state that accounts for both triplet state and non-fluorescing isomerized form. Although the molecular structure of Alexa Fluor 647 has not been made available yet, the FCS curves and fluorescence lifetimes clearly indicate that it has a carbocyanine structure, with a quantum yield in water solution of about 30% [34]. To the aim of the study reported here, and as far as the fluorescence brightness is concerned, this model will be sufficient. A more detailed description of the photokinetics of cyanine 5 dyes can be found in [35].

The photokinetic rates are noted as follows, and are summarized in appendix A : σI_e stands for the excitation rate, where σ denotes the excitation cross-section and I_e the excitation intensity. k_{rad} and k_{nrad} are the rate constants for radiative emission and non-radiative deexcitation from S_1 to the ground state. k_{isc} and k_d are the rate constants for inter-system crossing to the dark state and relaxation to the ground state respectively. The total deexcitation rate from the excited singlet state S_1 is noted as $k_{tot} = 1/\tau_{tot}$, where τ_{tot} is the excited state lifetime.

Under steady-state conditions, the fluorescence rate per molecule CRM is given by [36]

$$CRM = \kappa\,\phi\,\frac{\sigma I_e}{1+I_e/I_s} \tag{1}$$

where κ is the light collection efficiency, $\phi = k_{rad}/k_{tot}$ the quantum yield and $I_s = \frac{k_{tot}}{\sigma}\frac{1}{1+k_{isc}/k_d}$ is the saturation intensity.

To ease the understanding of our measurements, we introduce the emission rate $k_{em} = \kappa k_{rad}$, which denotes the effectively detected radiation rate by our instrument. Both radiative rate and collection efficiency are accounted into a single factor k_{em}. Eq. (1) then rewrites

$$CRM = \frac{k_{em}}{k_{tot}}\,\frac{\sigma I_e}{1+I_e/I_s} \tag{2}$$

#92310 - $15.00 USD Received 31 Jan 2008; revised 15 Feb 2008; accepted 15 Feb 2008; published 20 Feb 2008

In the low excitation regime $I_e \ll I_s$, Eq. (2) reduces to

$$CRM_{low} = \frac{k_{em}}{k_{tot}} \sigma I_e \qquad (I_e \ll I_s) \tag{3}$$

which indicates that the fluorescence rate per molecule is proportional to the excitation intensity and to the ratio of the detected emission rate to the overall decay rate. The fluorescence enhancement η_F can therefore be expressed as

$$\eta_{F,low} = \frac{CRM_{aper}}{CRM_{sol}} = \frac{\eta_{k_{em}}}{\eta_{k_{tot}}} \eta_{I_e} \qquad (I_e \ll I_s) \tag{4}$$

where $\eta_{k_{em}} = k_{em-aper}/k_{em-sol}$, $\eta_{k_{tot}} = k_{tot-aper}/k_{tot-sol}$ and $\eta_{I_e} = \sigma I_{e-aper}/\sigma I_{e-sol}$ are the enhancements in the collected emission rate, total decay rate and excitation rate.

In the saturation regime $I_e \gg I_s$, Eq. (2) reduces to

$$CRM_{sat} = \frac{k_{em}}{k_{tot}} \sigma I_s = \frac{k_{em}}{1 + k_{isc}/k_d} \qquad (I_e \gg I_s) \tag{5}$$

which indicates that the fluorescence rate per molecule at saturation is determined by the collected emission rate and the ratio k_{isc}/k_d. It is important to note that k_{isc}/k_d is proportional to the relative population of the dark state D once saturation is reached [32, 33]. We verified experimentally that the dark state fraction at fluorescence saturation was similar for all the nanoaperture diameters, as for the open solution. We therefore make the reasonable assumption that *at fluorescence saturation* the ratio k_{isc}/k_d is a constant set by the Alexa Fluor 647 properties, and that it is independent of the photonic environment. While computing the ratios of the fluorescence rates at saturation $\eta_{F,sat}$, the term $\frac{1}{1+k_{isc}/k_d}$ in Eq. (5) thus disappears, and one ends up with the simple expression

$$\eta_{F,sat} = \eta_{k_{em}} \qquad (I_e \gg I_s) \tag{6}$$

To characterize the fluorescence photokinetics enhancement induced by a single nanoaperture we will thus perform the following procedure :

- The fluorescence rates per molecule *CRM* are measured by FCS for increasing excitation powers in open solution and in single nanoapertures.
- The data points for *CRM* versus I_e are fitted according to Eq. (2). The ratio to the open solution gives η_F versus I_e. From the numerical fits, we infer the fluorescence enhancement at the limit below saturation $\eta_{F,low}$ and at saturation $\eta_{F,sat}$.
- According to Eq. (6), the value of $\eta_{F,sat}$ at saturation equals the emission rate enhancement $\eta_{k_{em}}$.
- The fluorescence decay rate k_{tot} is characterized by pulsed time-correlated measurements. The ratio of the results in the nanoaperture to the open solution gives $\eta_{k_{tot}}$.
- According to Eq. (4), the excitation rate enhancement is obtained as $\eta_{I_e} = \eta_{F,low}\,\eta_{k_{tot}}/\eta_{k_{em}}$.

As we will show below, this procedure turns out to be very efficient in discriminating the contributions of excitation and emission to the overall fluorescence process. The limit of this method is that all the presented results account for spatial averaging over all the possible molecular orientations and positions inside the analyzed volume. There is no sensitivity to individual

#92310 - $15.00 USD Received 31 Jan 2008; revised 15 Feb 2008; accepted 15 Feb 2008; published 20 Feb 2008

molecular trajectories or dipole orientations, but one ends up directly with global figures to characterize the (spatially averaged) emitted fluorescence. Besides, it is very difficult to reveal the physics underneath the emission rate $k_{em} = \kappa k_{rad}$ enhancement. Distinguishing between the contributions of the radiative rate k_{rad} and the collection efficiency κ remains a challenge, mainly because of the intrinsic difficulty to reliably measure a collection efficiency [22, 23]. Last, the fluorescence enhancement factors are spectrally averaged within the fluorescence bandpass detection window.

3. Materials and methods

Our experimental set-up is based on an inverted microscope with a NA= 1.2 water-immersion objective, allowing single aperture studies (Fig. 1). It combines on the same setup FCS and time-correlated lifetime measurements facilities, used to determine the complete photokinetics alteration in a nanoaperture following the procedure derived in section 2. We emphasize that for all experiments, a droplet of solution containing Alexa-Fluor 647 molecules is deposited on top of the aperture sample. The droplet acts as a reservoir of molecules, that are constantly diffusing inside the aperture, which strongly limits photobleaching effects.

3.1. Nanoapertures

Opaque gold films (thickness 200 nm) were coated on conventional microscope coverslips (thickness 150 μm) by thermal evaporation. A 15 nm thick chromium layer ensures adhesion between the gold film and the glass substrate. Circular apertures with diameters ranging from 80 nm to 310 nm were then directly milled by focused ion beam (FEI Strata DB235).

3.2. FCS measurements and analysis

For FCS measurements, the excitation is set to a CW HeNe laser operating at 633 nm. After a 50 μm confocal pinhole conjugated to the sample plane, the detection is performed by two avalanche photodiodes (Perkin-Elmer SPCM-AQR-13) with 670 ± 20 nm fluorescence band-pass filters. The fluorescence intensity fluctuations are analyzed by cross-correlating the signal of each photodiode with a ALV6000 hardware correlator. Each individual FCS measurement was obtained by averaging 5 runs of 10 s duration.

As an illustration, Fig. 2 presents typical correlograms $g^{(2)}(\tau)$ recorded in a 120 nm nanoaperture for three different excitation powers. The analysis of this FCS data relies on a numerical fit based on a three dimensional Brownian diffusion model [23, 36]:

$$g^{(2)}(\tau) = 1 + \frac{1}{N}\left(1 - \frac{\langle B\rangle}{\langle F\rangle}\right)^2 \left[1 + n_T \exp\left(-\frac{\tau}{\tau_{b_T}}\right)\right] \frac{1}{(1+\tau/\tau_d)\sqrt{1+s^2\,\tau/\tau_d}} \qquad (7)$$

where N is the total number of molecules, $\langle F\rangle$ the total signal, $\langle B\rangle$ the background noise, n_T the amplitude of the dark state population, τ_{b_T} the dark state blinking time, τ_d the mean diffusion time and s the ratio of transversal to axial dimensions of the analysis volume. Numerical fit of the FCS data following Eq. (7) provides the average number of molecules N which is used to compute the fluorescence count rate per molecule CRM.

The background noise $\langle B\rangle$ originates mainly from the back-reflected laser light and from gold autofluorescence. At 40 μW excitation powers, it typically amounts to $\langle B\rangle = 3$ kHz, which is almost negligible as compared to the count rates per molecule in the nanoapertures in the range 50-150 kHz (Fig. 3). In the configuration of Fig. 1, the aperture subwavelength diameter and the 200 nm gold thickness provide strong electromagnetic confinement at the aperture bottom. Therefore, fluorescence contribution from the pool of molecules above the nanoaperture was shown to be negligible [21].

#92310 - $15.00 USD Received 31 Jan 2008; revised 15 Feb 2008; accepted 15 Feb 2008; published 20 Feb 2008

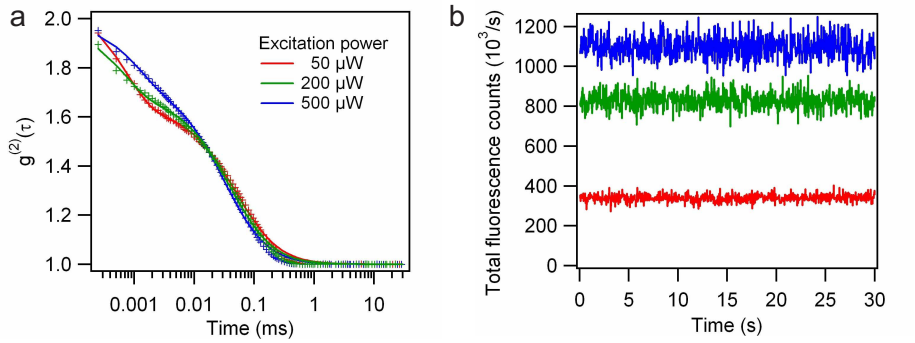

Fig. 2. (a) Typical fluorescence autocorrelations in a 120 nm aperture (crosses, raw data) and numerical fits according to Eq. (7) (lines). (b) Snapshot of the raw fluorescence signal corresponding to (a).

3.3. TCSPC measurements and fluorescence lifetime analysis

For TCSPC lifetime measurements, the excitation is turned to a picosecond laser diode operating at 636 nm (PicoQuant LDH-P-635 with PicoQuant driver SEPIA-II-SLM828). A single-mode optical fiber (Thorlabs P3-630A-FC-5) ensures a perfect spatial overlap between the pulsed laser diode and the CW HeNe laser. This guarantees the same excitation spot for FCS and TCSPC and almost same wavelength, contrary to previous experiments [21, 22]. For our measurements, the laser diode repetition rate was set to 80 MHz and the averaged excitation power measured at the microscope entrance port was 80 μW. Single photon detection is performed by a fast avalanche photodiode (Micro Photon Devices by PicoQuant MPD-5CTC, with timing jitter about 50 ps and active area 50 μm) with 670 ± 20 nm fluorescence bandpass filter. The photodiode output is coupled to a fast TCSPC module (PicoQuant PicoHarp 300, resolution per channel 4 ps). Overall, the temporal resolution of our setup is 120 ps FWHM. Switching from FCS to TCSPC is easily done by a set of two removable mirrors (Fig. 1(a)).

To measure the fluorescence decay rate, we use the following procedure that takes into account the limited resolution of our setup. Careful analysis of the instrument response function (IRF) (shown later on Fig. 5(a)) reveals a double exponential decay : $IRF(t) \propto A_1 \exp(-k_1 t) + A_2 \exp(-k_2 t)$ with $A_1 = 0.516$, $A_2 = 0.484$, $k_1 = 5.7\ 10^9\ \mathrm{s}^{-1}$ and $k_2 = 20.7\ 10^9\ \mathrm{s}^{-1}$. The output signal $O(t)$ of the TCSPC card corresponds to the convolution of the system IRF with the averaged fluorescence decay, which is assumed to be mono-exponential. Convolving a mono-exponential fluorescence decay with a double exponential IRF results in a triple exponential :

$$O(t) \propto (A_1 + A_2)\exp(-k_{tot}t) - A_1\exp(-k_1 t) - A_2\exp(-k_2 t) \tag{8}$$

where k_{tot} is the molecular total deexcitation rate, and A_1, A_2, k_1 and k_2 are fixed parameters set by the IRF analysis. While analyzing the experimental decay curves, k_{tot} is thus kept as the only free varying parameter. This procedure yields a fluorescence lifetime of 1.0 ns for Alexa Fluor 647 in open water solution, which corresponds well to the data in the literature [34].

4. Experimental results

To get a global picture of the fluorescence photokinetics alterations in a single nanoaperture, we carried extensive FCS experiments for aperture diameters ranging from 80 up to 310 nm. The excitation power was increased from 25 to 500 μW (the upper limit was set to avoid damaging the sample and photobleaching the dyes). Each correlation function was analyzed to compute

#92310 - $15.00 USD Received 31 Jan 2008; revised 15 Feb 2008; accepted 15 Feb 2008; published 20 Feb 2008

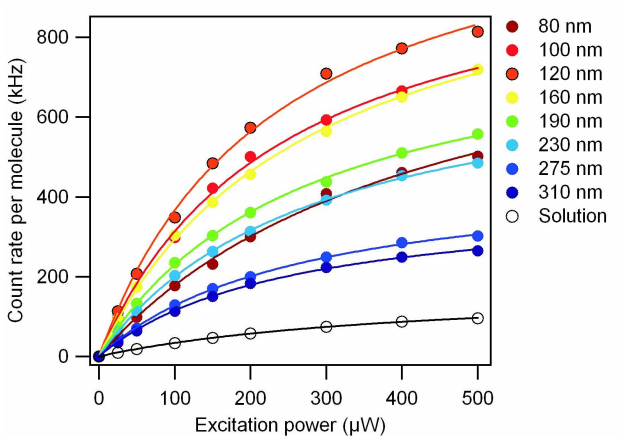

Fig. 3. Fluorescence rates per molecule *CRM* versus excitation power in open solution and in single nanoapertures. Circles are experimental data, lines are numerical fits using Eq. (2).

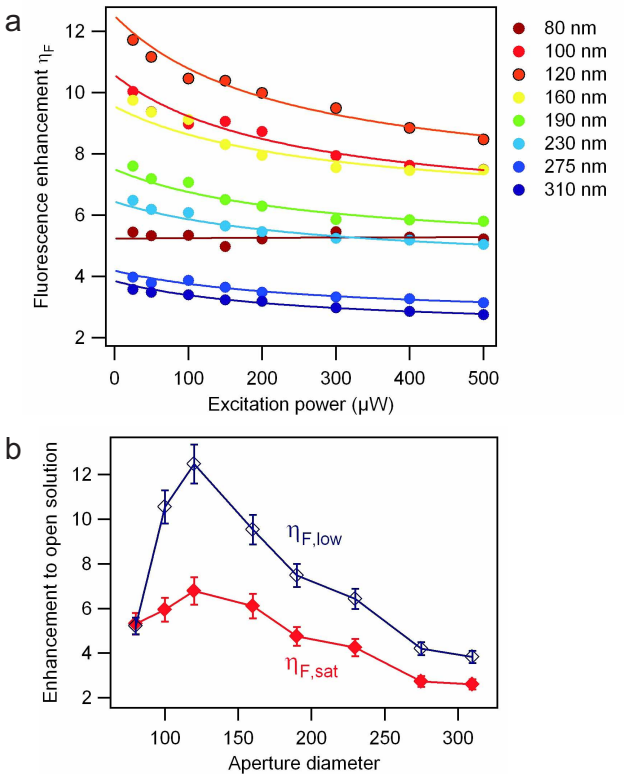

Fig. 4. (a) Fluorescence enhancement η_F derived from Fig. 3. (b) Fluorescence enhancement below saturation $\eta_{F,low}$ (empty markers) and at saturation $\eta_{F,sat}$ (filled markers) deduced from the numerical fits in Fig. 3 according to Eqs. (2), (4) and (6).

the average number of molecules *N* and fluorescence count rate per molecule *CRM*. Please note that special care has been taken to characterize the level of background noise and the dark state

#92310 - $15.00 USD Received 31 Jan 2008; revised 15 Feb 2008; accepted 15 Feb 2008; published 20 Feb 2008

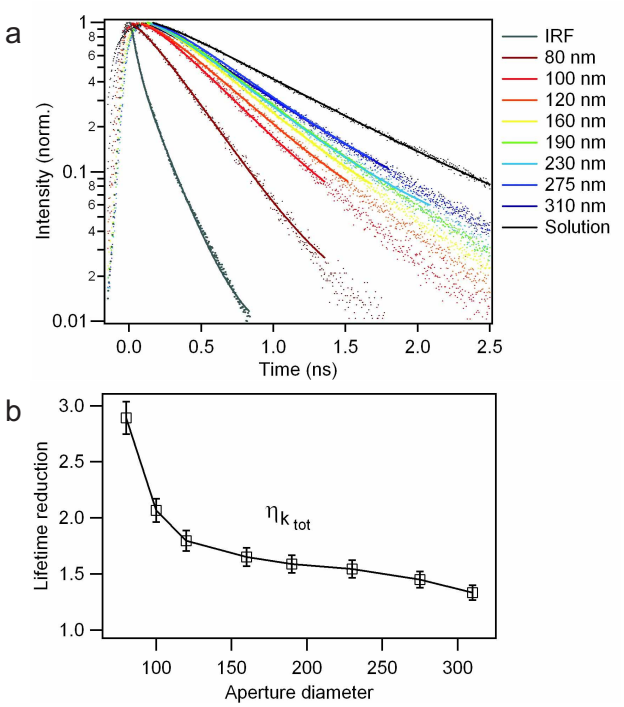

Fig. 5. (a) Normalized fluorescence decay traces measured in open solution (black dots) and in single nanoapertures. Dots are experimental data, lines are numerical fits following the procedure described in Sec. 3.3. The shorter decay trace (grey) is the overall instrument response function (IRF). (b) Fluorescence lifetime reduction versus the aperture diameter (as compared to open solution), deduced from the numerical fits in (a) using Eq. (8).

amplitude for each excitation power.

Figure 3 displays the evolution of the detected fluorescence rate per molecule *CRM* versus the excitation power for the different aperture diameters. Solid lines are numerical fits according to Eq. (2), which agree well to our experimental data. As the aperture diameter decreases, the fluorescence rate *CRM* increases before reaching an optimum for a diameter of 120 nm, which was previously assessed to give the largest fluorescence enhancement [23]. For smaller apertures (100 and 80 nm diameters), we show that *CRM* is decreased. Figure 3 also indicates that high count rates larger than 400,000 counts per second and per molecule are readily obtained in nanoapertures at high excitation power, while in open solution, the count rate saturates to values below 180,000 counts per second.

Count rates displayed on Fig. 3 were used to compute the corresponding fluorescence enhancement factors $\eta_F = CRM_{aper}/CRM_{sol}$. The results are displayed on Fig. 4(a) versus the excitation power, with an optimum diameter at 120 nm. Then, we use the numerical fits of *CRM* versus I_e according to Eqs. (2), (4) and (6) to infer the fluorescence enhancement well below saturation $\eta_{F,low}$ and at saturation $\eta_{F,sat}$. For clarity, we present these figures versus the aperture diameter in Fig. 4(b). The lower value for $\eta_{F,sat}$ as compared to $\eta_{F,low}$ results from the respective influence of the excitation intensity enhancement and lifetime reduction, as indicated in Eqs. (4) and (6). We point out that the reported fluorescence enhancement factors account for spectral averaging over the 650-690 nm detection window. Spectral dependence of the fluorescence enhancement has been investigated in [23], and was shown to cover the entire

#92310 - $15.00 USD Received 31 Jan 2008; revised 15 Feb 2008; accepted 15 Feb 2008; published 20 Feb 2008

dye emission spectrum with only slight spectral variations.

Along with the FCS measurements, for the same nanoaperture sample and the same Alexa Fluor 647 solution, we conducted TCSPC experiments to investigate the fluorescence lifetime alteration inside the nanoapertures. Figure 5(a) shows the measured fluorescence decay curves (dots) and their numerical fits (lines) for Alexa 647 molecules in single nanoapertures of diameters ranging from 80 up to 310 nm. As the aperture diameter is decreased, a clear reduction in the fluorescence lifetime is seen. To quantify this reduction, we fitted the data according to Eq. (8), and normalized the measured decay rate to the decay rate in open solution. This yields the ratio $\eta_{k_{tot}} = k_{tot-aper}/k_{tot-sol}$ displayed on Fig. 5(b). $\eta_{k_{tot}}$ increases as the aperture diameter is decreased, and as the metal comes closer to the average position of the molecules. We measure a clear lifetime reduction of about 3 for a 80 nm aperture.

5. Discussion

The different experimental results on Fig. 4 and 5 are now combined to estimate the alteration of the fluorescence photokinetics rates. We use the different steps described in section 2 : according to Eq. (6), the fluorescence enhancement at saturation $\eta_{F,sat}$ gives the emission rate enhancement $\eta_{k_{em}}$, which denotes the gain in radiative rate and collection efficiency. Then, following Eq. (4), the excitation rate enhancement is obtained from the fluorescence enhancement below saturation and the lifetime reduction as $\eta_{I_e} = \eta_{F,low}\,\eta_{k_{tot}}/\eta_{k_{em}}$. For completeness, all these results are presented on one single figure for each aperture diameter (Fig. 6(a) to (d)). We also compute the ratio $\eta_{k_{em}}/\eta_{k_{tot}}$ (Fig. 6(e)). This displays the gain in the factor $k_{em}/k_{tot} = \kappa k_{rad}/k_{tot} = \kappa\phi$ which is the product of the collection efficiency κ with the dye's quantum yield ϕ. Last, to comment on these results, we display the propagation constant γ of the fundamental guided mode inside an infinitely long aperture as a function of the aperture diameter (Fig. 6(f)), the aperture being filled with water [23].

A general comment on Fig. 6 is that the nanoaperture affects both emission and excitation in the fluorescence process. Both effects contribute to the large fluorescence enhancement observed. Hereafter, we will relate these effects to the local density of states (LDOS) increase induced by the nanoaperture. The global consideration of the graphs on Fig. 6 leads to the introduction of three regions as indicated by the dashed vertical lines on Fig. 6. Region (1) is for aperture diameters below 100 nm, region (2) for diameters between 100 and 175 nm, and region (3) stands for diameters above 175 nm. These regions are only intended to guide the following discussion, there are obviously no strict borders between them.

Starting from region (3), the general trend is an increase in the photokinetic rates as the aperture diameter is decreased. To compare with the propagation constant γ (Fig. 6(f)) we point out that in this region, the real part of the propagation constant is large while the imaginary part is low, corresponding to a propagative excitation field. As the aperture diameter is decreased, the imaginary part of the propagation constant grows, leading to more electromagnetic confinement at the aperture entrance. This translates into an increase in the emission enhancement along with the excitation enhancement (Fig. 6(b) and (d)).

On the other hand, region (1) shows a decrease in the fluorescence enhancement as the aperture diameter is reduced. This is linked to a large increase in k_{tot} (Fig. 6(c)), while at the same time, the emission and the excitation rates tend to decrease with the aperture diameter. Consequently, the apparent quantum yield k_{em}/k_{tot} decreases (Fig. 6(e)). These effects are strong evidences for fluorescence quenching, which we relate to a too close vicinity between the dyes and the metal. Let us also point out that region (1) corresponds to a large imaginary part of the propagation constant γ and thus to strongly evanescent fields inside the aperture and large losses. This contributes to the reduction in emission and excitation enhancement (Fig. 6(b) and (d)).

#92310 - $15.00 USD Received 31 Jan 2008; revised 15 Feb 2008; accepted 15 Feb 2008; published 20 Feb 2008

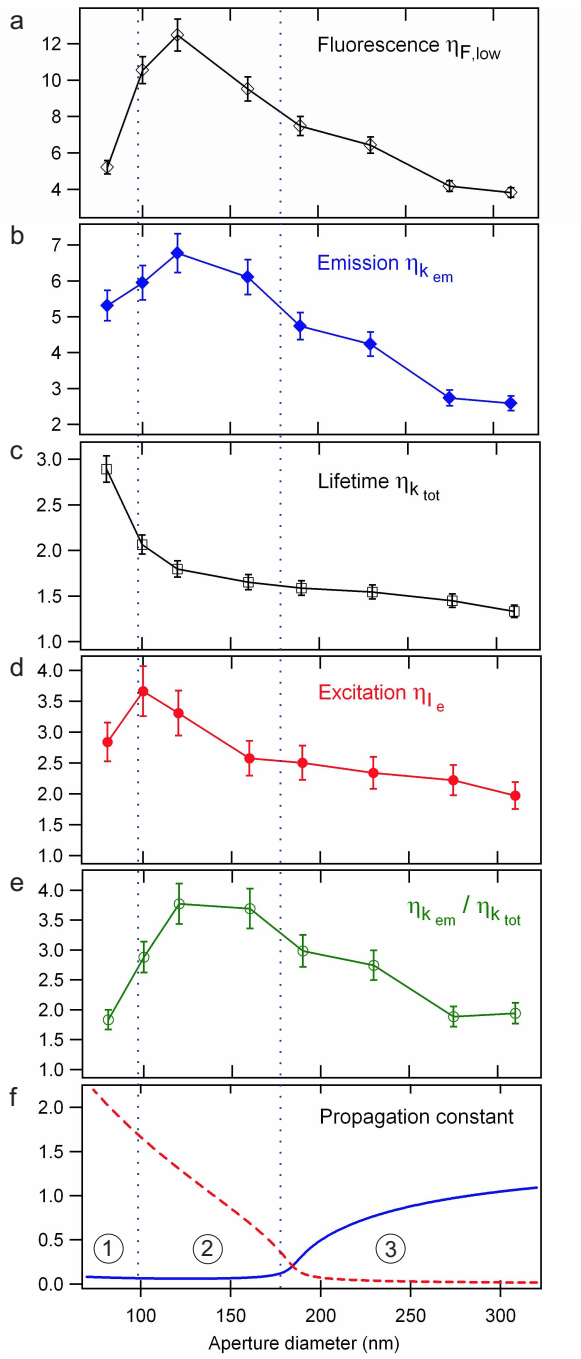

Fig. 6. Physical contributions to nanoaperture enhanced fluorescence, plotted versus the aperture diameter and normalized to the open solution case. (a) Fluorescence enhancement below saturation $\eta_{F,low}$, (b) Emission rate enhancement $\eta_{k_{em}}$, (c) Lifetime reduction $\eta_{k_{tot}}$, (d) Excitation enhancement η_{I_e}, (e) Ratio $\eta_{k_{em}}/\eta_{k_{tot}}$, (f) Propagation constant γ of the fundamental mode inside the aperture (solid line: real part, dashed line: imaginary part).

#92310 - $15.00 USD Received 31 Jan 2008; revised 15 Feb 2008; accepted 15 Feb 2008; published 20 Feb 2008

Last, region (2) appears as a trade-off between cases (1) and (3). This region is close to the cutoff of the fundamental mode that may propagate through the aperture and to the position where the group velocity is minimum (found for a diameter of 120 nm). These conditions lead to a maximum of the photonic density of states [1], and therefore to a maximum in the emission and excitation rates (Fig. 6(b) and (d)). Moreover, the metal-dielectric interface set by the aperture may allow fluorescence energy transferred to a surface plasmon to be coupled out into the radiated field at the aperture edge, contributing to the emission [2, 3]. At the same time, we infer that the molecules stay (on average) far enough from the metal layer, so that the relative influence of quenching to the metal is limited. This is supported by a plateau in the apparent quantum yield (Fig. 6(e)).

Finally, we point out that our experimental results stand in good agreement with the numerical predictions based on the finite elements method [37, 23] and differential theory [38].

6. Conclusion

We have detailed the influence of single nanometric apertures on the fluorescence of Alexa Fluor 647 molecules, and determined the respective contributions of excitation and emission in the observed enhanced fluorescence. The procedure has been conducted for a broad range of nanoapertures with diameters from 80 to 310 nm, which allowed us to discriminate between different physical effects and relate the photokinetics enhancements to the local photonic density of states. Let us emphasize that the characterization procedure combining FCS and TCSPC can be straightforwardly extended to other types of plasmonic nanostructures.

Finally, this study shows that nanoapertures bear many interesting properties for biophotonics, such as light localization, sub-femtoliter observation volume, and an increase in the excitation and emission yield. These properties are of great interest to increase the effectiveness of fluorescence-based single molecule detection.

Acknowledgments

The authors acknowledge stimulating discussions with S. Blair. This work has been funded by the French Agence Nationale de la Recherche under contract ANR-05-PNANO-035-01 “COEXUS” and ANR-07-NANO-006-03 “ANTARES”.

#92310 - $15.00 USD Received 31 Jan 2008; revised 15 Feb 2008; accepted 15 Feb 2008; published 20 Feb 2008

Appendix A: Fluorescence photokinetics notations

Symbol	Quantity
S_0	Molecular ground state
S_1	Excited single state
D	Dark state
σI_e	Excitation rate to S_1
σ	Excitation cross-section
I_e	Excitation intensity
k_{rad}	Rate constant for radiative emission
k_{nrad}	Rate constant for non-radiative deexcitation from S_1 to the ground state
k_{isc}	Rate constant for inter-system crossing to the dark state D
k_d	Rate constant for relaxation from D to S_0
k_{tot}	Total deexcitation rate from S_1: $k_{tot} = k_{rad} + k_{nrad} + k_{isc}$
τ_{tot}	Fluorescence lifetime $\tau_{tot} = 1/k_{tot}$
N	Average number of detected molecules
$\langle F \rangle$	Average total fluorescence signal per second
CRM	Fluorescence rate per molecule $CRM = \langle F \rangle / N$
κ	Collection efficiency
ϕ	Quantum yield $\phi = k_{rad}/k_{tot}$
I_s	Saturation intensity $I_s = k_{tot}/(\sigma(1 + k_{isc}/k_d))$
k_{em}	Effective emission rate $k_{em} = \kappa k_{rad}$
η_F	Fluorescence rate enhancement $\eta_F = CRM_{aper}/CRM_{sol}$
$\eta_{F,low}$	Fluorescence rate enhancement below saturation ($I_e \ll I_s$)
$\eta_{F,sat}$	Fluorescence rate enhancement at saturation ($I_e \gg I_s$)
$\eta_{k_{em}}$	Emission rate enhancement $\eta_{k_{em}} = k_{em-aper}/k_{em-sol}$
$\eta_{k_{tot}}$	Decay rate enhancement, lifetime reduction $\eta_{k_{tot}} = k_{tot-aper}/k_{tot-sol}$
η_{I_e}	Excitation rate enhancement $\eta_{I_e} = \sigma I_{e-aper}/\sigma I_{e-sol}$
η_κ	Collection efficiency enhancement $\eta_\kappa = \kappa_{aper}/\kappa_{sol}$

#92310 - $15.00 USD Received 31 Jan 2008; revised 15 Feb 2008; accepted 15 Feb 2008; published 20 Feb 2008